TENSORIAL CONVOLUTIVE BLIND SOURCE SEPARATION

Thanh Trung Le[⋆,‡], Karim Abed-Meraim[‡], Philippe Ravier[‡], Olivier Buttelli[‡], Ales Holobar[†]

[⋆] AVITECH Institute, VNU University of Engineering and Technology, Hanoi, Vietnam
[‡] PRISME Laboratory, University of Orléans, Orléans, France
[†] Institute of Computer Science, University of Maribor, Maribor, Slovenia

ABSTRACT

In this paper, we investigate the problem of convolutive blind source separation (BSS) via tensor decomposition. A fundamental link between convolutive BSS and block-term decomposition (BTD) is established, forming the basis for our novel tensor-based convolutive BSS method, namely TCBSS. Specifically, the proposed method offers a new effective approach for factorizing tensors under the BTD format where the loading factors are constrained to be identical. By leveraging second-order statistics of data observations, we construct a third-order tensor by stacking covariance matrices at different time lags, and then, apply TCBSS to identify the mixing process. Experimental results demonstrate the robust performance of TCBSS in addressing both BTD and convolutive BSS tasks, particularly when dealing with electromyography (EMG) signal decomposition.

Index Terms— Convolutive blind source separation, tensor decomposition, block term decomposition, second-order statistics, EMG decomposition.

1. INTRODUCTION

In this work, we consider the following convolutive blind source separation (BSS) model:

$$x_m(t) = \sum_{r=1}^{R} \sum_{\ell=0}^{L} a_{mr}(\ell) s_r(t-\ell), \quad t = 0, 1, \ldots, \qquad (1)$$

where $x_m(t)$ represents the data observed at the m-th sensor ($m = 1, 2, \ldots, M$); $s_r(t)$ is the r-th source signal ($r = 1, 2, \ldots, R$); $a_{mr}(\ell)$, $\ell = 0, 1, \ldots, L$ are coefficients of the impulse response from the r-th source to the m-th sensor, and $(L+1)$ is the maximum filter length. Given a set of data observations $\{x_m(t)\}$, it is desirable to identify the mixture process and recover the underlying source signals. In the literature, many effective methods have been proposed for BSS and convolutive BSS in particular. We refer the readers to [1–3] for good references.

Tensor decomposition (TD) has become a powerful processing tool for analyzing multidimensional data in both batch and adaptive settings [4–6]. With its capability to factorize multiway arrays (referred to as tensors) into basic components, TD has successfully demonstrated its applications in various signal processing problems and BSS tasks in particular [6, 7]. Noteworthy within this strategy are methodologies that leverage the classical canonical polyadic (CP) decomposition. This CP decomposition forms the basis for various tensor-based BSS algorithms, including [8–11], among others. High-order SVD has also been employed for BSS tasks, as demonstrated in works such as [12–14]. Another approach that holds promise in the context of tensor-based BSS is the $(L_r, L_r, 1)$-decomposition or LL1 decomposition [15–19]. The existing tensor-based BSS methods are, however, either designed for handling instantaneous BSS tasks rather than convolutive ones or applicable only to certain classes of source signals. One potential solution to address the former issue is to convert convolutive mixtures into instantaneous ones, often accomplished through frequency domain representations or transformations. Subsequently, current tensor-based methods can be used for source separation. However, this introduces a set of new issues, including complex-valued data, permutation and scaling indeterminacies, and the consistency of filter coefficients across frequencies, to name a few [3]. Hence, there is a need to readapt current tensor-based BSS algorithms to tackle them or, alternatively, to delve deeper into exploring novel methods that can bypass such issues.

In this paper, we adopt the latter strategy by presenting a new effective tensor-based method aimed at dealing with the convolutive BSS directly in time domain. In contrast to existing tensor-based BSS methods, our approach involves exploiting the merits of a special variant of the block term decomposition (BTD) where the loading factors are constrained to be identical. To elaborate, we establish a fundamental connection between convolutive BSS and this constrained BTD, forming the groundwork for our novel method called TCBSS. Specifically by exploiting second-order statistics, we first construct a third-order tensor by stacking a set of covariance matrices, and then, apply TCBSS to identify the mixing process and sources. Beyond its primary contribution to convolutive BSS, this paper also enriches the existing tensor literature by introducing an effective optimization approach for factorizing tensors under the BTD format.

2. PRELIMINARIES

2.1. Notations and Operations

We adopt a notation convention in which lowercase letters represent scalars (e.g., x), while boldface lowercase letters refer to

This work was supported by the European Pro-Athena program under grant No. 20-GURE-0012. Ales Holobar was supported by the Slovenian Research and Innovation Agency (Programme No. P2-0041).

vectors (e.g., $\mathbf{x}$). Matrices and tensors are denoted using boldface capital letters (e.g., $\mathbf{X}$) and bold calligraphic letters (e.g., $\boldsymbol{\mathcal{X}}$), respectively. The mode-n matricization of a tensor $\boldsymbol{\mathcal{X}}$ is denoted as $[\boldsymbol{\mathcal{X}}]_{(n)}$. The transpose operation is denoted as $(\cdot)^\top$, the pseudo-inverse as $(\cdot)^\#$, the Frobenius norm as $\|\cdot\|_F$, and the ℓ_2 norm as $\|\cdot\|_2$. The function "blkdiag$(\cdot)$" constructs a block diagonal matrix or tensor by arranging the inputs along its diagonal. Here, we present frequently-used mathematical operations in this paper.

The mode-n product of a tensor $\boldsymbol{\mathcal{X}} \in \mathbb{R}^{I_1 \times I_2 \times \cdots \times I_N}$ and a matrix $\mathbf{U} \in \mathbb{R}^{J_n \times I_n}$ returns a new tensor $\boldsymbol{\mathcal{Y}} = \boldsymbol{\mathcal{X}} \times_n \mathbf{U} \in \mathbb{R}^{I_1 \times \cdots \times J_n \times \cdots \times I_N}$ whose elements are given by

$$\boldsymbol{\mathcal{Y}}(i_1, \ldots, i_{n-1}, j_n, i_{n+1}, \ldots, i_N) = \sum_{i_n=1}^{I_n} \boldsymbol{\mathcal{X}}(i_1, \ldots, i_{n-1}, i_n, i_{n+1}, \ldots, i_N)\mathbf{U}(j_n, i_n). \quad (2)$$

If $\boldsymbol{\mathcal{Y}} = \boldsymbol{\mathcal{X}} \times_n \mathbf{U}$ then $[\mathbf{Y}]_{(n)} = \mathbf{U}[\mathbf{X}]_{(n)}$.

The Kronecker product of two matrices $\mathbf{A} \in \mathbb{R}^{M \times N}$ and $\mathbf{B} \in \mathbb{R}^{P \times Q}$ is defined as

$$\mathbf{A} \otimes \mathbf{B} = \begin{bmatrix} a_{11}\mathbf{B} & \ldots & a_{1N}\mathbf{B} \\ \vdots & \ddots & \vdots \\ a_{M1}\mathbf{B} & \ldots & a_{MN}\mathbf{B} \end{bmatrix}. \quad (3)$$

The bloc-wise Kronecker product of $\mathbf{A} = [\mathbf{A}_1, \ldots, \mathbf{A}_R]$ and $\mathbf{B} = [\mathbf{B}_1, \ldots, \mathbf{B}_R]$ results in

$$\mathbf{A} \otimes_b \mathbf{B} = \big[\mathbf{A}_1 \otimes \mathbf{B}_1, \ldots, \mathbf{A}_R \otimes \mathbf{B}_R\big]. \quad (4)$$

2.2. Type-2 BTD

The type-2 BTD is a variant of the block term decomposition (BTD) method [20]. It aims to factorize a third-order tensor $\boldsymbol{\mathcal{X}} \in \mathbb{R}^{I \times J \times K}$ into a set of low multilinear-rank components $\{\boldsymbol{\mathcal{X}}_r\}_{r=1}^R$, which can be expressed as follows

$$\boldsymbol{\mathcal{X}} = \sum_{r=1}^{R} \boldsymbol{\mathcal{X}}_r = \sum_{r=1}^{R} \boldsymbol{\mathcal{G}}_r \times_1 \mathbf{A}_r \times_2 \mathbf{B}_r. \quad (5)$$

Here, $\boldsymbol{\mathcal{G}}_r \in \mathbb{R}^{L_r \times M_r \times K}$ represents the core tensor of the r-th component $\boldsymbol{\mathcal{X}}_r$, while the loading factors $\mathbf{A}_r \in \mathbb{R}^{I \times L_r}$ and $\mathbf{B}_r \in \mathbb{R}^{J \times M_r}$ are full column rank matrices. Since (5) is trilinear in $\mathbf{A} = [\mathbf{A}_1, \mathbf{A}_2, \ldots, \mathbf{A}_R]$, $\mathbf{B} = [\mathbf{B}_1, \mathbf{B}_2, \ldots, \mathbf{B}_R]$, and $\boldsymbol{\mathcal{G}} = \text{blkdiag}(\boldsymbol{\mathcal{G}}_1, \boldsymbol{\mathcal{G}}_2, \ldots, \boldsymbol{\mathcal{G}}_R)$, its computation follows the common alternating least-squares (ALS) approach [21]. Also, the type-2 BTD is essential unique under mild conditions [20].

To support our algorithm development in Section 4, we present three mode-n matrix representations of $\boldsymbol{\mathcal{X}}$:

$$[\boldsymbol{\mathcal{X}}]_{(1)} = \mathbf{A}\big[[\boldsymbol{\mathcal{G}}_1 \times_2 \mathbf{B}_1]_{(1)}^\top, \ldots, [\boldsymbol{\mathcal{G}}_R \times_2 \mathbf{B}_R]_{(1)}^\top\big]^\top, \quad (6)$$

$$[\boldsymbol{\mathcal{X}}]_{(2)} = \mathbf{B}\big[[\boldsymbol{\mathcal{G}}_1 \times_1 \mathbf{A}_1]_{(2)}^\top, \ldots, [\boldsymbol{\mathcal{G}}_R \times_1 \mathbf{A}_R]_{(2)}^\top\big]^\top, \quad (7)$$

$$[\boldsymbol{\mathcal{X}}]_{(3)} = \big[[\boldsymbol{\mathcal{G}}_1^{(l)}]_{(3)}, \ldots, [\boldsymbol{\mathcal{G}}_R^{(l)}]_{(3)}\big]\big(\mathbf{B} \otimes_b \mathbf{A}\big)^\top. \quad (8)$$

3. LINK BETWEEN CONVOLUTIVE BSS AND CONSTRAINED TYPE-2 BTD

In this section, we present a fundamental link between convolutive BSS and a constrained type-2 BTD factorization.

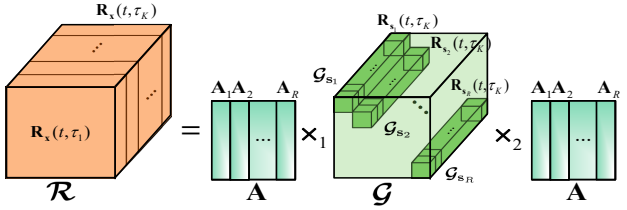

Fig. 1: Constrained Type-2 BTD based Convolutive BSS

As suggested in [3,22], we can reformulate the convolutive data model (1) into an instantaneous one as follows

$$\mathbf{x}(t) = \mathbf{A}\mathbf{s}(t), \quad (9)$$

where

$$\mathbf{s}(t) = [s_1(t), \ldots, s_1(t-(L+L')+1), \ldots, s_R(t), \ldots, s_R(t-(L+L')+1)]^\top \in \mathbb{R}^{R(L+L')}, \quad (10)$$

$$\mathbf{x}(t) = [x_1(t), \ldots, x_1(t-L'+1), \ldots, x_M(t), \ldots, x_M(t-L'+1)]^\top \in \mathbb{R}^{ML'}, \quad (11)$$

with an extension factor for data observations $L' \geq 1$ and the new mixture $\mathbf{A} \in \mathbb{R}^{ML' \times R(L+L')}$ is given by

$$\mathbf{A} = \begin{bmatrix} \mathbf{A}_{11} & \ldots & \mathbf{A}_{1R} \\ \vdots & \ddots & \vdots \\ \mathbf{A}_{M1} & \ldots & \mathbf{A}_{MR} \end{bmatrix} \quad \text{with} \quad (12)$$

$$\mathbf{A}_{mr} = \begin{bmatrix} a_{mr}(0) & \ldots & a_{mr}(L) & \ldots & \mathbf{0} \\ & \ddots & \ddots & \ddots & \\ \mathbf{0} & & a_{mr}(0) & \ldots & a_{mr}(L) \end{bmatrix}. \quad (13)$$

For short, we denote $L_{\text{add}} = L + L'$.

In many applications, individual source signals are temporally coherent while maintaining their mutual independence, such as [22–24]. Specifically, the correlation between the two sources s_i and s_j (with $i \neq j$) follows $\mathbb{E}\{s_i(t)s_j(t-\tau)\} = 0$, for all τ. In such cases, the correlation matrix corresponding to (9) is expressed as

$$\begin{aligned} \mathbf{R}_{\mathbf{x}}(t,\tau) &\triangleq \mathbb{E}\{\mathbf{x}(t)\mathbf{x}(t-\tau)^\top\} = \mathbf{A}\mathbb{E}\{\mathbf{s}(t)\mathbf{s}(t-\tau)^\top\}\mathbf{A}^\top \\ &= \mathbf{A}\begin{bmatrix} \mathbf{R}_{\mathbf{s}_1}(t,\tau) & & & \\ & \mathbf{R}_{\mathbf{s}_2}(t,\tau) & & \mathbf{0} \\ & & \ddots & \\ \mathbf{0} & & & \mathbf{R}_{\mathbf{s}_R}(t,\tau) \end{bmatrix}\mathbf{A}^\top \\ &\triangleq \mathbf{A}\text{blkdiag}\big(\{\mathbf{R}_{\mathbf{s}_r}(t,\tau)\}_{r=1}^R\big)\mathbf{A}^\top. \end{aligned} \quad (14)$$

For multiple time lags $\{\tau_i\}_{i=1}^K$, we obtain

$$\begin{cases} \mathbf{R}_{\mathbf{x}}(t,\tau_1) &= \mathbf{A}\text{blkdiag}\big(\{\mathbf{R}_{\mathbf{s}_r}(t,\tau_1)\}_{r=1}^R\big)\mathbf{A}^\top, \\ &\vdots \\ \mathbf{R}_{\mathbf{x}}(t,\tau_K) &= \mathbf{A}\text{blkdiag}\big(\{\mathbf{R}_{\mathbf{s}_r}(t,\tau_K)\}_{r=1}^R\big)\mathbf{A}^\top. \end{cases} \quad (15)$$

Particularly by stacking $\{\mathbf{R}_{\mathbf{x}}(t,\tau_k)\}_{k=1}^K$ and $\{\mathbf{R}_{\mathbf{s}}(t,\tau_k)\}_{k=1}^K$ consecutively within the third mode of $\boldsymbol{\mathcal{R}} \in \mathbb{R}^{ML' \times ML' \times K}$ and $\boldsymbol{\mathcal{G}} \in \mathbb{R}^{RL_{\text{add}} \times RL_{\text{add}} \times K}$, we derive the following representation

$$\boldsymbol{\mathcal{R}} = \boldsymbol{\mathcal{G}} \times_1 \mathbf{A} \times_2 \mathbf{A} = \sum_{r=1}^{R} \boldsymbol{\mathcal{G}}_{\mathbf{s}_r} \times_1 \mathbf{A}_r \times_2 \mathbf{A}_r, \quad (16)$$

where $\mathcal{G}_{\mathbf{s}_r}(:,:,k) = \mathbf{R}_{\mathbf{s}_r}(t,\tau_k)$ and $\mathbf{A}_r = [\mathbf{A}_{1r}^\top, \ldots, \mathbf{A}_{Mr}^\top]^\top$ is the r-th block column of $\mathbf{A}$. See Fig. 1 for an illustration.

We can see that (16) represents a variant of the type-2 BTD in (5), where the loading factors $\mathbf{A}$ and $\mathbf{B}$ are constrained to be identical. Interestingly, (16) is also essentially unique under mild conditions, as highlighted by Proposition 1. In particular, the estimate $\bar{\mathbf{A}}$ of $\mathbf{A}$ is unique up to trivial indeterminacies, i.e., $\bar{\mathbf{A}} = \mathbf{A}\mathbf{\Pi}\mathbf{\Lambda}$ where $\mathbf{\Pi}$ is a block permutation matrix and $\mathbf{\Lambda}$ is a square nonsingular block-diagonal matrix.

Proposition 1 (Uniqueness)**.** *If $ML' \geq RL_{\text{add}}$, $K \geq 3$, and $\mathcal{G}$ is generic,*[1] *then* (16) *is essentially unique.*

This result is a corollary of Theorem 6.1 in [20]. Consequently, by employing the constrained type-2 BTD analysis, we can directly identify the mixing process in convolutive BSS. In next section, we introduce an effective optimization framework designed to deal with (16) in an efficient way.

4. OPTIMIZATION FRAMEWORK

The type-2 BTD factorization (16) can be represented by the following optimization

$$\min_{\mathcal{G},\mathbf{A},\mathbf{B}} \Big\| \mathcal{R} - \sum_{r=1}^{R} \mathcal{G}_{\mathbf{s}_r} \times_1 \mathbf{A}_r \times_2 \mathbf{B}_r \Big\|_F^2 \quad \text{s.t.} \quad \mathbf{A} = \mathbf{B}. \tag{17}$$

where $\mathbf{A} = [\mathbf{A}_1, \ldots, \mathbf{A}_R]$ and $\mathbf{B} = [\mathbf{B}_1, \ldots, \mathbf{B}_R]$. Here, we can formulate the augmented Lagrangian function for the constrained minimization (17) as follows

$$\mathcal{L}(\mathcal{G},\mathbf{A},\mathbf{B},\mathbf{U}) = \min_{\mathcal{G},\mathbf{A},\mathbf{B}} \Big\| \mathcal{R} - \sum_{r=1}^{R} \mathcal{G}_{\mathbf{s}_r} \times_1 \mathbf{A}_r \times_2 \mathbf{B}_r \Big\|_F^2 + \frac{\rho}{2}\big\|\mathbf{B} - \mathbf{A} + \mathbf{U}\big\|_F^2 - \frac{\rho}{2}\big\|\mathbf{U}\big\|_F^2, \tag{18}$$

where $\mathbf{U}$ is the "scaled" dual variable and $\rho > 0$ is a regularized parameter. To find the stationary point of $\mathcal{L}(\cdot)$, we propose the following iteration procedure.

while stopping criteria are not met **do**

$$\mathbf{A}^{(l)} = \underset{\mathbf{A}}{\operatorname{argmin}} \Big\| \mathcal{R} - \sum_{r=1}^{R} \mathcal{G}_{\mathbf{s}_r}^{(l-1)} \times_1 \mathbf{A}_r \times_2 \mathbf{B}_r^{(l-1)} \Big\|_F^2 + \frac{\rho}{2}\Big\|\mathbf{B}^{(l-1)} - \mathbf{A} + \mathbf{U}^{(l-1)}\Big\|_F^2 \tag{19a}$$

$$\mathbf{B}^{(l)} = \underset{\mathbf{B}}{\operatorname{argmin}} \Big\| \mathcal{R} - \sum_{r=1}^{R} \mathcal{G}_{\mathbf{s}_r}^{(l-1)} \times_1 \mathbf{A}_r^{(l)} \times_2 \mathbf{B}_r \Big\|_F^2 + \frac{\rho}{2}\Big\|\mathbf{B} - \mathbf{A}^{(l)} + \mathbf{U}^{(l-1)}\Big\|_F^2 \tag{19b}$$

$$\mathcal{G}^{(l)} = \underset{\mathcal{G}}{\operatorname{argmin}} \Big\| \mathcal{R} - \sum_{r=1}^{R} \mathcal{G}_{\mathbf{s}_r} \times_1 \mathbf{A}_r^{(l)} \times_2 \mathbf{B}_r^{(l)} \Big\|_F^2 \tag{19c}$$

$$\mathbf{U}^{(l)} = \mathbf{Z}^{(l-1)} + \mathbf{B}^{(l)} - \mathbf{A}^{(l)} \tag{19d}$$

$$\alpha_l = \frac{1 + \sqrt{1 + 4\alpha_{l-1}^2}}{2} \tag{19e}$$

$$\mathbf{Z}^{(l)} = \mathbf{U}^{(l)} + \frac{\alpha_{l-1} - 1}{\alpha_l}\big(\mathbf{U}^{(l)} - \mathbf{U}^{(l-1)}\big) \tag{19f}$$

$l = l + 1$

end

At $l = 0$, matrices $\mathbf{A}^{(0)}$, $\mathbf{B}^{(0)}$, $\mathbf{U}^{(0)}$, $\mathbf{Z}^{(0)}$, and tensor $\mathcal{G}^{(0)}$ are initialized at random, while the value of α_0 is set to 1.

The proposed procedure (19) relies on the duality theory for convex optimization. The main objective is to minimize the augmented Lagrangian function $\mathcal{L}(\cdot)$ w.r.t. $\mathbf{A}$, $\mathbf{B}$, and $\mathcal{G}$, respectively, while keeping the dual variable $\mathbf{U}$ constant. It involves three sub-problems (19a), (19b), and (19c) whose closed-form solutions are provided below. The dual function, represented as $f(\mathbf{U}) = \min_{\mathcal{G},\mathbf{A},\mathbf{B}} \mathcal{L}(\cdot)$, needs to be maximized w.r.t. $\mathbf{U}$. Inspired by the work [25], we introduce two auxiliary variables $\mathbf{Z}^{(l)}$ and α_l to accelerate the iteration procedure. The inclusion of (19d), (19e), and (19f) results in an accelerated augmented Lagrangian variant which can offer superior speed and estimation accuracy, as compared with state-of-the-art methods, please see Fig. 2 for an example.

Due to the space limitation, we omit the detailed derivations of (19a), (19b), and (19c). Here, we present their closed-form solutions $\mathbf{A}^{(l)}$, $\mathbf{B}^{(l)}$, and $\mathcal{G}^{(l)}$, as follows

$$\mathbf{A}^{(l)} = \Big(\boldsymbol{\mathcal{R}}_{(1)}\mathbf{W}_A^{(l)^\top} + \rho\big(\mathbf{B}^{(l-1)} + \mathbf{U}^{(l-1)}\big)\Big)\Big(\mathbf{W}_A^{(l)}\mathbf{W}_A^{(l)^\top} + \rho\mathbf{I}_{RL_{\text{add}}}\Big)^{-1}, \tag{20}$$

$$\mathbf{B}^{(l)} = \Big(\boldsymbol{\mathcal{R}}_{(2)}\mathbf{W}_B^{(l)^\top} + \rho\big(\mathbf{U}^{(l-1)} - \mathbf{A}^{(l)}\big)\Big)\Big(\mathbf{W}_B^{(l)}\mathbf{W}_B^{(l)^\top} + \rho\mathbf{I}_{RL_{\text{add}}}\Big)^{-1}, \tag{21}$$

$$\Big[[\mathcal{G}_{\mathbf{s}_1}^{(l)}]_{(3)}, \ldots, [\mathcal{G}_{\mathbf{s}_R}^{(l)}]_{(3)}\Big] = \boldsymbol{\mathcal{R}}_{(3)}\big((\mathbf{B}^{(l)} \otimes_b \mathbf{A}^{(l)})^\top\big)^{\#}, \tag{22}$$

where $\mathbf{W}_A^{(l)}$ and $\mathbf{W}_B^{(l)}$ are given by

$$\mathbf{W}_A^{(l)} = \Big[\big[\mathcal{G}_{\mathbf{s}_1}^{(l-1)} \times_2 \mathbf{B}_1^{(l-1)}\big]_{(1)}^\top, \ldots, \big[\mathcal{G}_{\mathbf{s}_R}^{(l-1)} \times_2 \mathbf{B}_R^{(l-1)}\big]_{(1)}^\top\Big]^\top,$$

$$\mathbf{W}_B^{(l)} = \Big[\big[\mathcal{G}_{\mathbf{s}_1}^{(l-1)} \times_1 \mathbf{A}_1^{(l)}\big]_{(2)}^\top, \ldots, \big[\mathcal{G}_{\mathbf{s}_R}^{(l-1)} \times_1 \mathbf{A}_R^{(l)}\big]_{(2)}^\top\Big]^\top.$$

Stopping Criteria: Our procedure stops either upon convergence, or reaching the maximum number of iterations $I_{\text{stop}} = 100$, or by meeting the following criteria

$$\big\|\mathbf{A}^{(l)} - \mathbf{B}^{(l)}\big\|_F \leq \varepsilon_{\text{pri}}, \quad \big\|\rho(\mathbf{A}^{(l)} - \mathbf{A}^{(l-1)})\big\|_F \leq \varepsilon_{\text{dual}}, \tag{23}$$

where

$$\varepsilon_{\text{pri}} = \epsilon_{\text{abs}}\sqrt{MRL'L_{\text{add}}} + \epsilon_{\text{rel}} \max\Big\{\big\|\mathbf{A}^{(l)}\big\|_2, \big\|\mathbf{B}^{(l)}\big\|_2\Big\},$$

$$\varepsilon_{\text{dual}} = \epsilon_{\text{abs}}\sqrt{MRL'L_{\text{add}}} + \epsilon_{\text{rel}}\big\|\rho\mathbf{U}^{(l)}\big\|_2.$$

Here, $\epsilon_{\text{abs}} > 0$ and $\epsilon_{\text{rel}} > 0$ represent the absolute and relative tolerance, respectively. In practice, we can set $\rho = 1, \epsilon_{\text{abs}} = 10^{-4}$ and $\epsilon_{\text{rel}} = 10^{-2}$ for reasonable performance.

Computational Complexity: At each iteration, the updates for both $\mathbf{A}^{(l)}$ in (20) and $\mathbf{B}^{(l)}$ in (21) share the same computational process. This requires $\mathcal{O}\big(M^2L'^2L_{\text{add}}RK + ML'L_{\text{add}}^2R^2K + L_{\text{add}}^3R^3\big)$ flops. For computing $\mathcal{G}^{(l)}$ defined in (22), the complexity is $\mathcal{O}\big(M^2L'^2L_{\text{add}}^2RK + M^2L'^2RL_{\text{add}}^2 \min(M^2L'^2, RL_{\text{add}}^2)\big)$ flops. The computations required for updating $\mathbf{U}^{(l)}$, $\mathbf{Z}^{(l)}$, and α_l are inexpensive, with respective complexities of $\mathcal{O}(ML'RL_{\text{add}})$, $\mathcal{O}(ML'RL_{\text{add}})$, and $\mathcal{O}(1)$. As mentioned in Proposition 1, satisfying the uniqueness condition demands $ML' \geq RL_{\text{add}}$. Accordingly, the overall complexity of TCBSS is $\mathcal{O}\big(M^2L'^2\ L_{\text{add}}^2R\max(K, L_{\text{add}}^2R) + L_{\text{add}}^3R^3\big)$ flops at each iteration.

[1] We call a tensor generic when its elements are drawn from a continuous probability density function.

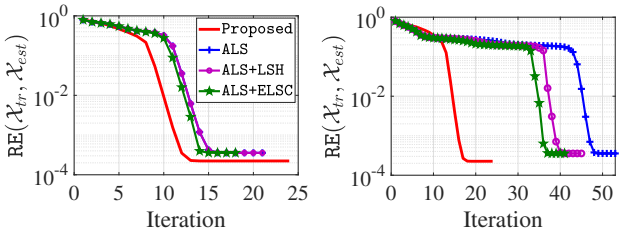

(a) $M = 10, R = 2, L = 2$ (b) $M = 50, R = 5, L = 4$

Fig. 2: Convergence rate of type-2 BTD algorithms: $K = 100$, and $\sigma_n = 10^{-2}$.

Table 1: Running time of type-2 BTD algorithms

Method	ALS	ALS+LSH	ALS+ELSC	TCBSS
Fig. 2(a)	0.22(s)	0.24(s)	0.25(s)	0.17(s)
Fig. 2(b)	0.36(s)	0.39(s)	0.43(s)	0.28(s)

5. SIMULATIONS

We evaluate the performance of TCBSS by (i) analyzing its convergence rate for type-2 BTD factorization, and (ii) applying it to the problem of EMG decomposition. Our experiments are implemented in MATLAB on a computer with an Intel core i7, 3.00GHz CPU and 16GB of RAM.

Experiment 1: Tensor Decomposition. We first demonstrate its effectiveness in the context of constrained type-2 BTD factorization. To illustrate this, we generate a third-order tensor $\boldsymbol{\mathcal{X}} \in \mathbb{R}^{M\times M\times K}$ as follows

$$\boldsymbol{\mathcal{X}} = \boldsymbol{\mathcal{X}}_{tr} + \sigma_n \boldsymbol{\mathcal{N}} = \sum_{r=1}^{R} \boldsymbol{\mathcal{G}}_r \times_1 \mathbf{A}_r \times_2 \mathbf{A}_r + \sigma_n \boldsymbol{\mathcal{N}}. \quad (24)$$

Here, the elements of $\boldsymbol{\mathcal{G}}_r \in \mathbb{R}^{L\times L\times K}$, $\boldsymbol{\mathcal{N}} \in \mathbb{R}^{M\times M\times K}$, and $\mathbf{A}_r \in \mathbb{R}^{M\times L_r}$ are derived from random Gaussian variables with zero mean and unit variance. The parameter $\sigma_n > 0$ is introduced to control the noise level. To measure the estimation accuracy, we use the following relative error metric

$$\mathrm{RE}(\boldsymbol{\mathcal{X}}_{tr}, \boldsymbol{\mathcal{X}}_{est}) = \|\boldsymbol{\mathcal{X}}_{tr} - \boldsymbol{\mathcal{X}}_{est}\|_F / \|\boldsymbol{\mathcal{X}}_{tr}\|_F, \quad (25)$$

where $\boldsymbol{\mathcal{X}}_{est}$ is the reconstructed tensor. Fig. 2 and Tab. 1 show the performance of TCBSS as compared with the widely-used ALS method [21] and its variants: ALS+LSH [26] and ALS+ELSC [27]. We can see that the proposed algorithm not only achieves faster convergence but also provides improved estimation accuracy.

Experiment 2: EMG Decomposition. We apply TCBSS to the problem of EMG decomposition and compare its performance with other tensor-based BSS algorithms, namely PARAFAC-SD [11] and LL1-segmentation [18].

Synthetic EMG signals are simulated using the convolutive model (1), where $a_{mr}(\ell)$ represents the action potential (AP) of the r-th motor unit (MU) at the m-th sensor. The duration of the APs is 35 (i.e., $L = 34$). The source $s_r(t) = \sum_j \delta(t - \psi_{rj})$ corresponds to the spike train of the r-th MU, featuring spikes at times ψ_{rj} with $\delta(\cdot)$ being the Dirac delta function. In particular, the m-th measurement $\mathbf{x}_m$ is formulated as

$$\mathbf{x}_m = \sum_{r=1}^{R} \mathbf{y}_{mr} = \sum_{r=1}^{R} \mathbf{a}_{mr} * \mathbf{s}_r, \quad (26)$$

see Fig. 3 for an illustration. The objective of the EMG decomposition is to identify the underlying sources $\{\mathbf{y}_{mr}\}_{m=1,r=1}^{M,R}$ (spike trains $\{\mathbf{s}_r\}_{r=1}^{R}$ and MUs $\{\mathbf{a}_{mr}\}_{m=1,r=1}^{M,R}$) from $\{\mathbf{x}_m\}_{m=1}^{M}$. We refer the reader to [28, 29] for further details.

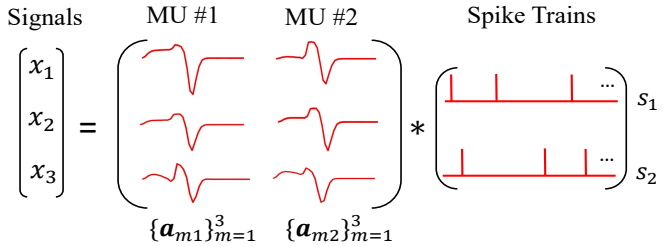

Fig. 3: Synthetic EMG signals: Convolutive mixture model with 3 measurements and 2 sources.

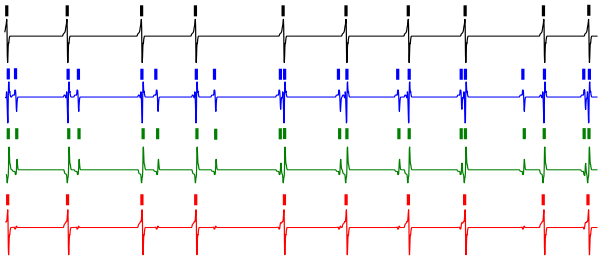

Fig. 4: EMG decomposition results (i.e., spike train (▮) and waveform (–)) related to the first component $\mathbf{y}_{11} = \mathbf{a}_{11} * \mathbf{s}_1$: Ground truth (▬), estimates by PARAFAC-SD (▬), LL1-segmentation (▬), and the proposed TCBSS (▬).

For this task, we generate three measurements ($M = 3$), comprising of two sources ($R = 2$) with an excitation level set at 5% of the maximum voluntary contraction. The sampling frequency is $f_s = 2048$ Hz. To satisfy the uniqueness condition $ML' \geq R(L + L')$ in Proposition 1, we set the extension factor L' of TCBSS to $2L$. Additionally, we set the number of time lags K to 30. Once obtaining the mixing matrix, the underlying sources are obtained up to an unknown filter via the ordinary least-squares method. Then, we identify the timings of activations of each MU, thanks to the form of spike (impulse) trains. The decomposition results related to the first EMG source are depicted in Fig. 4. We can see that TCBSS is capable of reconstructing EMG sources albeit with small artifacts present. TCBSS also demonstrates improved performance as compared to PARAFAC-based and LL1-based methods.

6. CONCLUSIONS

In this paper, we presented a connection between convolutive blind source separation (BSS) and type-2 block-term decomposition (BTD). Consequently, we introduced a novel and efficient method called TCBSS to address the constrained type-2 BTD, effectively dealing with convolutive BSS. The results indicated that TCBSS outperformed the "workhorse" alternating least-squares (ALS) method and its variants for the BTD task in terms of both convergence rate and estimation accuracy. The effectiveness of TCBSS for the problem of convolutive BSS was then illustrated with EMG decomposition.

7. REFERENCES

[1] P. Comon and C. Jutten, *Handbook of Blind Source Separation: Independent Component Analysis and Applications*, 2010.

[2] G. R. Naik and W. Wang, *Blind Source Separation: Advances in Theory, Algorithms and Applications*, 2014.

[3] M. S. Pedersen, J. Larsen, U. Kjems, and L. C. Parra, "A survey of convolutive blind source separation methods," *Multichannel Speech Processing Handbook*, pp. 114–126, 2007.

[4] T. G. Kolda and B. W. Bader, "Tensor decompositions and applications," *SIAM Rev.*, vol. 51, no. 3, pp. 455–500, 2009.

[5] L. T. Thanh, K. Abed-Meraim, N. L. Trung, and A. Hafiane, "A contemporary and comprehensive survey on streaming tensor decomposition," *IEEE Trans. Knowl. Data Eng.*, vol. 35, no. 11, pp. 10 897–10 921, 2023.

[6] A. Cichocki, D. Mandic, L. De Lathauwer *et al.*, "Tensor decompositions for signal processing applications: From two-way to multiway component analysis," *IEEE Signal Process. Mag.*, vol. 32, no. 2, pp. 145–163, 2015.

[7] G. Chabriel, M. Kleinsteuber, E. Moreau *et al.*, "Joint matrices decompositions and blind source separation: A survey of methods, identification, and applications," *IEEE Signal Process. Mag.*, vol. 31, no. 3, pp. 34–43, 2014.

[8] L. De Lathauwer, J. Castaing, and J.-F. Cardoso, "Fourth-order cumulant-based blind identification of underdetermined mixtures," *IEEE Trans. Signal Process.*, vol. 55, no. 6, pp. 2965–2973, 2007.

[9] L. De Lathauwer and J. Castaing, "Blind identification of underdetermined mixtures by simultaneous matrix diagonalization," *IEEE Trans. Signal Process.*, vol. 56, no. 3, pp. 1096–1105, 2008.

[10] M. Sørensen and L. De Lathauwer, "Blind signal separation via tensor decomposition with Vandermonde factor: Canonical polyadic decomposition," *IEEE Trans. Signal Process.*, vol. 61, no. 22, pp. 5507–5519, 2013.

[11] D. Nion, K. N. Mokios, N. D. Sidiropoulos, and A. Potamianos, "Batch and adaptive PARAFAC-based blind separation of convolutive speech mixtures," *IEEE Trans. Audio Speech Lang. Process.*, vol. 18, no. 6, pp. 1193–1207, 2010.

[12] L. De Lathauwer *et al.*, "Blind source separation by higher-order singular value decomposition," in *Proc. Eur. Signal Process. Conf.*, 1994, pp. 175–178.

[13] V. Zarzoso, A. Nandi, and E. Bacharakis, "Maternal and foetal ECG separation using blind source separation methods," *Math. Med. Biol.*, vol. 14, no. 3, pp. 207–225, 1997.

[14] V. D. Vrabie *et al.*, "Multicomponent wave separation using HOSVD/unimodal-ICA subspace method," *Geophysics*, vol. 71, no. 5, pp. V133–V143, 2006.

[15] L. De Lathauwer, "Block component analysis, a new concept for blind source separation," in *Int. Conf. Latent Var. Anal. Signal Sep.*, 2012, pp. 1–8.

[16] ——, "Blind separation of exponential polynomials and the decomposition of a tensor in rank-(L_r,L_r,1) terms," *SIAM J. Matrix Anal. Appl.*, vol. 32, no. 4, pp. 1451–1474, 2011.

[17] O. Debals, M. Van Barel, and L. De Lathauwer, "Löwner-based blind signal separation of rational functions with applications," *IEEE Trans. Signal Process.*, vol. 64, no. 8, pp. 1909–1918, 2016.

[18] M. Boussé, O. Debals, and L. De Lathauwer, "A tensor-based method for large-scale blind source separation using segmentation," *IEEE Trans. Signal Process.*, vol. 65, no. 2, pp. 346–358, 2017.

[19] N. Govindarajan, E. N. Epperly, and L. De Lathauwer, "(L_r,L_r,1)-decompositions, sparse component analysis, and the blind separation of sums of exponentials," *SIAM J. Matrix Anal. Appl.*, vol. 43, no. 2, pp. 912–938, 2022.

[20] L. De Lathauwer, "Decompositions of a higher-order tensor in block terms – Part II: Definitions and uniqueness," *SIAM J. Matrix Anal. Appl.*, vol. 30, no. 3, pp. 1033–1066, 2008.

[21] L. De Lathauwer and D. Nion, "Decompositions of a higher-order tensor in block terms – Part III: Alternating least squares algorithms," *SIAM J. Matrix Anal. Appl.*, vol. 30, pp. 1067–1083, 2008.

[22] H. Bousbia-Salah, A. Belouchrani, and K. Abed-Meraim, "Jacobi-like algorithm for blind signal separation of convolutive mixtures," *Electr. Lett.*, vol. 37, no. 16, p. 1, 2001.

[23] A. Belouchrani, K. Abed-Meraim, J.-F. Cardoso, and E. Moulines, "A blind source separation technique using second-order statistics," *IEEE Trans. Signal Process.*, vol. 45, no. 2, pp. 434–444, 1997.

[24] K. Abed-Meraim, Y. Xiang, J. H. Manton, and Y. Hua, "Blind source-separation using second-order cyclostationary statistics," *IEEE Trans. Signal Process.*, vol. 49, no. 4, pp. 694–701, 2001.

[25] M. Kang, M. Kang, and M. Jung, "Inexact accelerated augmented Lagrangian methods," *Comput. Optim. Appl.*, vol. 62, pp. 373–404, 2015.

[26] M. Rajih, P. Comon, and R. A. Harshman, "Enhanced line search: A novel method to accelerate PARAFAC," *SIAM J. Matrix Anal. Appl.*, vol. 30, no. 3, pp. 1128–1147, 2008.

[27] D. Nion and L. De Lathauwer, "An enhanced line search scheme for complex-valued tensor decompositions. Application in DS-CDMA," *Signal Process.*, vol. 88, no. 3, pp. 749–755, 2008.

[28] C. J. De Luca, A. Adam, R. Wotiz *et al.*, "Decomposition of surface EMG signals," *J. Neurophysiol.*, vol. 96, no. 3, pp. 1646–1657, 2006.

[29] D. Farina and A. Holobar, "Characterization of human motor units from surface EMG decomposition," *Proc. IEEE*, vol. 104, no. 2, pp. 353–373, 2016.